



SRTTU

Journal of Computational and Applied Research  
in Mechanical Engineering

jcarme.sru.ac.ir

JCARME

ISSN: 2228-7922

**Research paper****Simulation of blood flow in the abdominal aorta considering penetration into the organs using pore network model****S. Karimi<sup>a,\*</sup>, M. Dadvar<sup>b</sup> and B. Dabir<sup>b</sup>**<sup>a</sup>*Department of Chemical Engineering, Jundi-Shapur University of Technology, Dezful, Iran*<sup>b</sup>*Department of Chemical Engineering, Amirkabir University of Technology, Tehran, Iran***Article info:****Article history:**

Received: 28/08/2019

Revised: 21/04/2020

Accepted: 25/04/2020

Online: 28/04/2020

**Keywords:**

Abdominal Aorta,

Non-newtonian blood  
flow,

Outlet boundary,

Condition,

Porous media.

**\*Corresponding author:**[s.karimi@jsu.ac.ir](mailto:s.karimi@jsu.ac.ir)**Abstract**

One of the critical limitations of studies on cardiovascular blood flow simulation is to determine outlet boundary conditions accurately. In the present study, for the first time, pore network model is proposed as a useful technique to take into account interaction between blood flow and other body organs. Thus body organs are simulated by pore network model. Thanks to the method, pressure distribution among the porous medium of organ is determined and consequently the required boundary conditions are obtained for the simulation of arterial blood flow. The comparison between permeability resulted from developed model and experimental results shows that the difference is about 3% for the assumption of non-Newtonian blood flow through organ. This indicates the pore network model can accurately simulate velocity and pressure in the organs. Afterwards, a 3D patient-specific abdominal aorta was simulated under the proposed outlet boundary condition. The maximum deviation of predicted pressure from physiological data is 11.14% near the systole instant. Generally, the predicted pressure and velocity profiles are evident that the model can adequately simulate the blood flow through the arteries which feed main organs.

**1. Introduction**

Applying proper boundary conditions is one of the challenging concepts in numerical simulation of aortic blood flow [1-6], in particular, when numerical model includes aortic branches that feed body organs. In this condition, interaction between blood flow and organs should be considered in order to model the blood flow more accurately. Previously, the most common

outlet boundary conditions in CFD models of large arteries were constant or time-dependent either pressure or velocity. Due to vascular downstream resistance built up by organs, modeling have some limitations when those boundary conditions are used. Specifically, if equal pressures are applied to various artery outlets then it is imposed an inaccurate flow split [7-9]. Moreover, calculated blood pressure would not be in physiological range. Therefore,

simulation results could not be utilized in cases which flow distribution and pressure field are unknown [10, 11]. Furthermore applying time-dependent velocity or pressure boundary conditions demands to determine velocity or pressure profiles experimentally while the data is not usually available. Hence data for outlet boundary condition is required which is not only consist the realistic conditions but also not necessitate to take them from several points of artery. Gallo et al. [12] showed that using wrong MRI results as inlet or outlet boundary condition how much can impact on the simulation results. Additionally, Shahcheraghi et al. [13] injected a non-interactive tracer to an artery and showed that in hemodynamic studies, interaction between blood flow and other body parts should be considered as outlet and inlet boundary conditions.

Shalman et al. [14], in their numerical modeling of a stenosed artery, assumed that vascular bed, the sum of the blood vessels supplying an organ, is a porous medium characterized by permeability constant. They showed that the porous medium acts as hemodynamic resistance of vascular beds. But their study was limited to a stenosed artery and the utilized permeability constant is not generalized to other parts. Kim et al. [15] proposed an Augmented Lagrangian formulation to constrain the velocity profile at the inlet or outlet boundaries. Their formula has two drawbacks: first, the complexity of the blood flow is not considered and second, the velocity magnitude could not be calculated by it. The pseudo-organ boundary condition theory was developed by Park et al. [2] for the first time. The theory considered various body organs fed by aortic artery as porous media. Park et al. [2] assumed that each pseudo-organ has cylindrical shape with  $15\text{mm}$  in length and a diameter twice that of feeding artery. Although the pseudo-organ idea was useful in representing the interaction between blood flow and organs, but it needs to improve in many aspects. For example, it is not realistic to use a same permeability for all organs regarding the different nature of them.

In general, most body organs can be assumed as porous media with regard to the blood vessel distribution among them. In the present study, a pore network model is developed to take into

account the interaction. The body organs are simulated by pore network model for the first time. Firstly, the organs are modeled as a 3D porous media. Then, the obtained results are applied in arterial blood flow model as outlet boundary conditions. After that, a three-dimensional simulation of a patient-specific abdominal aorta is carried out using the obtained outlet boundary conditions. Finally, blood flow distribution throughout the major branch vessels and pressure field are calculated.

The paper consists of two parts. First, a 3D pore network model were conducted to take into account the interaction between blood flow and body organs, with the results that a correlation function between inlet velocity and pressure into the organs was found. We claim that this correlation can be used as a proper outlet boundary condition in artery blood flow simulations. Second, to evaluate the claim, a 3D patient-specific abdominal aorta was simulated under the proposed boundary condition.

## 2. Method

### 2.1. Developing pore network model

In the first part of the paper, pore network model was used to simulate the porous media of liver. In this model, transport equations were written for each pore. Then, the problem was solved in whole porous media scale considering the connectivity between pores and applying the equations. It is assumed that each pore is a continuum medium and the continuity of the whole medium is controlled by percolation theory [16-18]. As a result, pressure distribution was determined and based on that, it is obtained the required boundary conditions in artery blood flow simulation. The reason for choosing liver tissue is the availability of experimental data on its permeability.

Figs. 1(a and b) show a schematic of pores and nodes in two dimensional square and three dimensional cube ideal networks having coordinate number 4 and 6, respectively. Coordinate number, denoted by  $z$ , is the number of pores connected to each node of the network. We assumed that pores act as connections between nodes and no significant reaction occurs in them. Each pore throat is assumed to be cylindrical which we assigned an effective radius with the same length  $H$ .

It was considered that the effective radii,  $r$ , of the pores are distributed according to a probability density function (PDF),  $f(r)$ . Due to the lack of detailed data on body organs, the following PDF was used [16, 18, 19]:

$$f(r) = \frac{r - r_m}{(r_a - r_m)^2} \exp\left(-\frac{1}{2} \left(\frac{r - r_m}{r_a - r_m}\right)^2\right) \quad (1)$$

where  $r_a$  and  $r_m$  are average and minimum radius of pore, respectively. The probability of being pore radius equal  $r$ , can be calculated by the PDF as follows:

$$\int_{r_m}^r f(r) dr = R \quad (2)$$

where  $R$  is a random number between zero and one. According to Eq. (2), the pore radius was determined by creating a random number and integrating the PDF.

The coordination number is between 4 and 8 for the most porous media. If the coordination number of a network is different from the one of an ideal network, it can be created by a randomized procedure. Thus a fraction  $p_b$  of the pores was selected randomly and their effective radii were set to zero [17] where:

$$p_b = 1 - \frac{\langle z \rangle}{z} \quad (3)$$

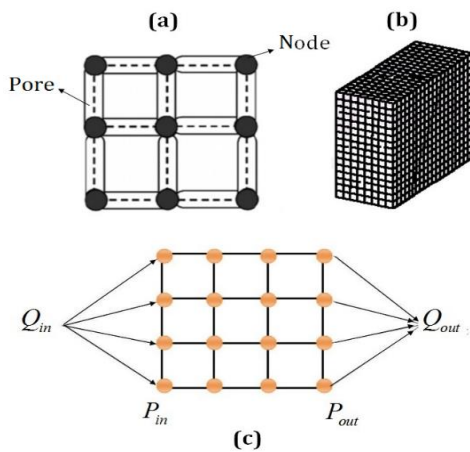


**Fig. 1.** A schematic of pores and nodes in ideal networks (a) two dimensional square network (b) three dimensional cube network; (c) a schematic diagram of a pore network model.

where  $z$  is 4 or 6 in two dimensional square or three dimensional cube network, respectively,

and  $\langle z \rangle$  is the average coordination number of the disordered network.

To determine the pressure and flow fields in the constructed pore network, it was assumed that the blood flow is laminar. Hence, assuming Newtonian viscosity, the volumetric flow rate,  $Q_{ij}$ , in each pore  $ij$  of the network is given by Hagen-Poiseuille equation:

$$Q_{ij} = (P_i - P_j) \frac{\pi r_{ij}^4}{8\mu H} \quad (4)$$

where  $r_{ij}$  is the radius of pore  $ij$ ,  $H$  is the pore length,  $\mu$  is the blood viscosity and  $P_i$  and  $P_j$  are the inlet and outlet pressure of the pore, respectively. In addition, the total volume of the fluid entering any node  $i$  of the network must be equal to the volume of the fluid leaving that node because of the lack of reaction in the network. Thus we have:

$$\sum_{ij} Q_{ij} = 0 \quad (5)$$

where the sum is over all bonds  $ij$  connected to node  $i$ . Writing down Eq. (5) for every node of the network results in a set of simultaneous linear equations for the nodal pressure. Monte Carlo method was used to minimize uncertainty in the results, which is due to the selected random number in calculating pore radius (Eq. 2). The calculations were repeated for ten different random networks with equal PDF and coordination number. Then the average of the obtained results was accepted as the final result. Finally, the organ permeability was determined by Darcy equation based on the calculated nodal pressures.

Due to time consuming of the computation and the necessity of using a high performance computer, the whole porous medium is not simulated and the calculation is done over a small part of the one. But the results could be independent of the network size if a proper one is selected and the results are generalized to the whole network. Hence, the volumetric flow rate was corrected as follows:

$$Q_{sample} = Q_{actual} \frac{\rho V_{sample}}{M_{sample}} \quad (6)$$

$$u = \frac{Q_{sample}}{A_{sample}} \quad (7)$$

where  $Q_{actual}$  and  $Q_{sample}$  are the volumetric flow rate through the whole medium and the small model, respectively,  $\rho$  is the organ density,  $V_{sample}$  is the volume of the small model,  $M_{sample}$  is the total mass of the organ,  $u$  is the apparent velocity and  $A_{sample}$  is the cross section area of the small model. Fig. 1(c) shows a schematic diagram of the network model. As illustrated in Fig. 1(c), the blood flow enters the primary nodes with a specified volumetric flow rate, then flows throughout the network and finally leaves it.

The average weight of an adult liver is about 1.4kg with the density of  $1000kg/m^3$  and the entering blood flow is  $1450ml/min$  [20]. The assumed flow is uniform and blood is a Newtonian fluid. The following initial data set: average pore radius,  $r_a = 10 \times 10^{-6}m$ , minimum pore radius,  $r_m = 4 \times 10^{-6}m$ , pore length,  $H = 1.2 \times 10^{-3}m$ , blood viscosity,  $\mu = 0.0035Pa.s$ , volumetric blood flow,  $Q = 2.4167 \times 10^{-5}m^3/s$ , and outlet pressure,  $P_{out} = 10mmHg$ . It is noted, in the pore network model, the outlet pressure was fixed to be  $10mmHg$  (according to physiological data). Therefore, changing inlet pressure causes to change the pressure gradient within the model. The three dimensional simulation was done in different conditions and the permeability was calculated by changing the number of nodes, coordination number and average pore radius. The calculated permeability was compared with the reported one by Debbaut et al. [21]. They injected a polymer through a human liver. All vessels were clamped and the injected fluid polymerized during a short period of time. Then, the liver tissue was removed to generate the polymerized vascular replica. The produced polymer was scanned with a CT scanner to obtain the 3D geometry. And the average

permeability is determined by computational fluid dynamics method.

In the present study a FORTRAN program was developed to simulate organs with pore network model and it was carried out on a Pentium IV processor running at 2500MHz. In the program, the Bi-conjugate Gradient method was utilized to solve the set of linear equations.

Besides, according to studies which show that the blood is a non-Newtonian fluid [22] especially in small blood vessels, in the present work, the pore network model was also developed, assuming Carreau-Yasuda non-Newtonian rheology [23]:

$$\mu(\dot{\gamma}) = \mu_{\infty} + (\mu_0 - \mu_{\infty}) \left[ 1 + (\lambda \dot{\gamma})^{\alpha} \right]^{\frac{(n-1)}{\alpha}} \quad (8)$$

where  $\mu$  is the apparent blood viscosity,  $\dot{\gamma}$  is the shear rate and  $\lambda$  is the relaxation time constant in second. It is noted that  $\lim_{\dot{\gamma} \rightarrow \infty} \mu(\dot{\gamma}) = \mu_{\infty}$  and  $\lim_{\dot{\gamma} \rightarrow 0} \mu(\dot{\gamma}) = \mu_0$  indicating at the high shear rates, the fluid acts like a Newtonian fluid with viscosity  $\mu_{\infty}$  whereas at low shear rates, the fluid acts as a Newtonian fluid with viscosity  $\mu_0$ . The parameters  $\alpha$ ,  $n$  and  $\lambda$  control how the fluid behaves in the non-Newtonian regime between these two asymptotic viscosities. Experimental studies [24-26] show that  $\lambda = 8.2s$ ,  $\mu_{\infty} = 0.0035Pa.s$ ,  $n = 0.2128$  and  $\alpha = 0.64$  are the best choice for non-Newtonian blood flow. In this case, the Hagen-Poiseuille equation was replaced with Navier–Stokes equation (convective form)[27].

## 2.2. Obtaining proper boundary conditions

After constructing the network model and verifying it by comparison its permeability with experimental data, it is time to find the outlet boundary condition of the artery which is the organ inlet. For this purpose, inlet pressure to the organ was selected which it is a function of inlet velocity especially in pulsatile blood flow. Thus, the equation of pulsatile flow rate was given as an input data to the computer code developed in previous section and accordingly pressure was calculated versus velocity. Then the calculated

pressure was verified by comparison with the available experimental data.

Because there was no data about renal tissue, it was assumed to be similar to liver. According to the assumption, developed model for liver is applicable to renal. If you have experimental results about the renal permeability (similar to the data obtained by Debaut et al. [21]), the same procedure described for liver in previous section should be followed to find the proper number of nodes, coordination number and average pore radius. Therefore, the new pore network model could be used for renal artery simulation.

### 2.3. Three dimensional modeling of abdominal aorta

In the second part of the paper, the pressure obtained from pore network model was applied as outlet boundary condition in the simulation of blood flow through abdominal artery. To do this, a 3D model shown in Fig. 2 was created from images acquired from a healthy 56 years old female volunteer (Rasoul Akram hospital, Tehran, Iran). The geometry was reconstructed from the grayscale CT scan images. The volunteer did not suffer from any arterial disease at the time of images acquisition. The distance between consecutive slices was 0.8mm. The contours extracted from CT images were connected to build a 3D hollow surface for the lumen of aorta using the computer package 3D-Doctor V4.0. Computer Aided Design (CAD) programs, 3Ds Max Design and SOLIDWORKS, were employed to remove unwanted vessels and organs and converting the set of nodes to surfaces, respectively. In the final stage, the 3D volume was trimmed and meshed by ANSYS V.13. The geometry included one inlet boundary and four outlet boundary which are right and left renal and iliac arteries. Inferior mesenteric artery has been neglected since less than 7% of the volumetric flow is diverted to it [28-31].

Mesh independence analysis was performed on the results of steady state simulation at the average inlet velocity with the Newtonian rheology. The grid was refined until the independence of results on grid size was achieved for average pressure distribution. The results are summarized in Table 1. According to Table 1, the final grid contained 208817 hybrid elements comprised of tetrahedral and hexahedral elements.

The time-dependent flow of blood was modeled by solving 3D incompressible Navier–Stokes equations,

$$\rho \left[ \frac{\partial u}{\partial t} + (u \cdot \nabla) u \right] = -\nabla p - \nabla \cdot \tau \tag{9}$$

$$\nabla u = 0 \tag{10}$$

where  $u$  is velocity vector,  $t$  is time,  $\rho$  is density of fluid,  $p$  is hydrostatic pressure and  $\tau$  is shear stress. It is noted that the arterial wall was assumed as a rigid boundary in the present paper.

The aortic blood flow was simulated with  $\rho=1050\text{ kg/m}^3$  and constant viscosity  $\mu=0.0035\text{ kg/m.s}$ , using the finite volume method (FVM) provided in the computer package ANSYS-FLUENT v.13. A time-dependent inlet flow velocity profile was applied for the pulsatile flow simulation [32-35], as shown in Fig. 3. The equation of the volumetric flow rate was calculated assuming the average diameter of the renal artery 3.5mm .

The obtained equation by the pore network model (pressure versus velocity) was used as renal outlet boundary conditions and the outflow boundary condition was imposed at the iliac outlets. The flow is assumed as laminar. SIMPLE algorithm was selected for the pressure–velocity coupling.

A first order upwind scheme was applied to solve the momentum equations. For all the calculations, the convergence criterion for the residuals of continuity and velocity components was determined to be less than  $10^{-4}$ . For the unsteady three dimensional calculations, a fully implicit scheme with uniform time step 0.01s was used and simulations were carried out over at least two complete cycles to achieve a periodic solution.

**Table 1.** The results of mesh independence test.

Number of nodes	Average pressure (mmHg)
33355	101.17
112483	100.26
208817	99.71
292235	99.63

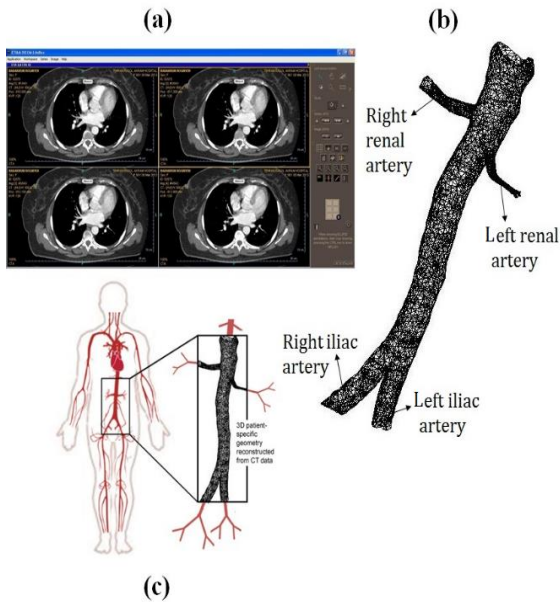


**Fig. 2.** The geometry of the realistic abdominal aorta, (a) Examples of taken CT scan images, (b) The reconstructed model that has been meshed, (c) Schematic representation of the part of arterial tree that is studied.

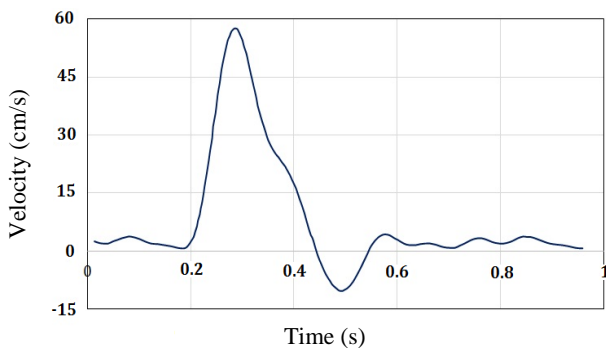


**Fig. 3.** Velocity pulse of the abdominal aorta inlet [32, 33].

### 3. Results and discussion

#### 3.1. Pore network model

In the first part of the paper, we tried to find the proper network model that mimics the liver tissue. It means to find number of nodes, coordination number and average pore radius so that the model permeability is close to its experimental value.

To specify the best number of nodes, the 3D pore network model has been implemented with 30 to 50 nodes, assuming the coordination number 5. Since the nodes number indicates the size of the selected network, a number should be selected as

the optimum one which the obtained results are independent of the network size. Fig. 4(a), shown the average permeability calculated by different number of nodes, indicates more number of nodes, less permeability. There is a dramatic downturn for less number of nodes. But there is not much change in high numbers so that the permeability of the network with 50 nodes is 1.52% less than the one with 40 nodes. Since more time is spent on the computation with the higher number of nodes, therefore 40 nodes is selected as the optimum one.

Reducing the coordination number causes eliminating a number of pores, and consequently changing the network shape. Therefore, organ permeability is directly affected by coordination number. Fig. 4(b) shows the calculated permeability at different coordination number while keeping the number of nodes constant 40. As we expected, it rises significantly with increasing the coordination number. On the other hand, the calculated average permeability differs from the one reported by Debbaut et al. [21] ( $2.3167 \times 10^{-14} m^2$ ).

Hence the next parameter, the average pore radius, should be monitored.

It is reported the obtained results from the pore network model with 40 nodes, coordination number 5 and different pore radius in Table 2. According to the table, pore radius variation has more effect on estimated permeability, so that increasing pore radius enhances it. The comparison between tabulated results and the reported one by Debbaut et al. [21] shows the pore radius  $3.3 \times 10^{-6} m$  is an appropriate choice in the modeling of liver.

According to the above results, in order to model the porous medium of liver, the optimum choice of the number of nodes, coordination number and average pore radius are 40, 5 and  $3.3 \times 10^{-6} m$ , respectively. Using these parameters, the simulated mean permeability coefficients on the Newtonian and non-Newtonian assumption are  $2.6002 \times 10^{-14} m^2$  and  $2.3922 \times 10^{-14} m^2$ , respectively. These results are comparable with the experimental data of Debbaut et al. [21] that is  $2.3167 \times 10^{-14} m^2$ . The comparative study indicates that the non-Newtonian model achieves more satisfactory results than the Newtonian model. This result was expected

because blood behaves like a non-Newtonian fluid at low shear rates and during its flow through small blood vessels.

### 3.2. Outlet boundary condition

Now we are trying to find answer to question that how the obtained results from the pore network model can be employed to derive outlet boundary condition. Thus using the developed pore network model, the inlet pressure to model is calculated at different inlet velocities. The results are displayed in Fig. 5 for both Newtonian and non-Newtonian blood rheology. As indicated in Fig. 5, for Newtonian model, the inlet pressure versus velocity changes linearly. The result of curve fitting is:

$$P(u) = 1.3041u + 31.335 \quad (11)$$

where  $u$  is the velocity in  $cm/s$  and  $P$  is the pressure in  $mmHg$ . Moreover, in the case of non-Newtonian blood rheology, the following equation was determined by curve fitting techniques:

$$P(u) = a_1 \sin(b_1u + c_1) + a_2 \sin(b_2u + c_2) + a_3 \sin(b_3u + c_3) + a_4 \sin(b_4u + c_4) + a_5 \sin(b_5u + c_5) \quad (12)$$

The constants of Eq. (12) are listed in Table 3. In order to verify the method, in Table 4 the predicted pressure by Eqs. (11) and (12) are compared with experimental data in different velocities in renal artery. Table 4 shows that results of the pore network model are in good agreement with the reported experimental results, so that the error does not exceed 14%. Moreover, using Carreau-Yasuda model, the average error is less which is predictable due to the nature of blood in small blood vessels of the organ. The agreement of the results confirms that Eqs. (11) and (12) can be used as the outlet boundary condition in aortic blood flow simulation.

### 3.3. Abdominal aorta flow

Three dimensional pulsatile flow in a patient specific abdominal artery are simulated using the obtained outlet boundary condition via the pore

network model. The results of flow simulations are presented for the peak systole.

In order to evaluate whether use of the pore network model is appropriate or not, the obtained pressure and velocity at various sections of the model are compared with the experimental data [32, 33]. The values are reported in Table 5. The high similarity of both results (predicted by modified outlet boundary condition and physiological data) confirms the convenience of using the pore network model to consider the interaction between blood flow and organs. As indicated in Table 4, the derived equation (Eq. (12)) shows its maximum deviation from physiological data is 11.14% near the systole instant ( $V \cong 43.76 cm/s$ ).

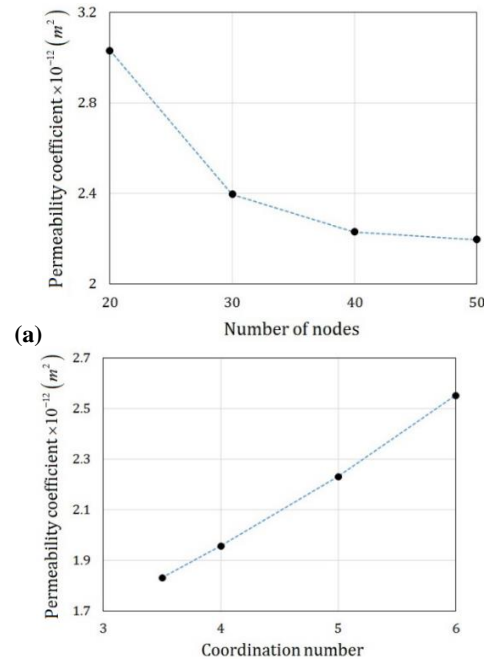


**Fig. 4.** Average permeability calculated by (a) different number of nodes, (b) different coordination number while keeping the number of nodes constant of 40.

**Table 2.** Mean permeability coefficient calculated in average pore radius by pore network model.

Average pore radius ( $m$ )	Mean permeability coefficient ( $m^2$ )
$3.3 \times 10^{-6}$	$2.6002 \times 10^{-14}$
$5 \times 10^{-6}$	$1.2076 \times 10^{-13}$
$10 \times 10^{-6}$	$2.2310 \times 10^{-12}$
$20 \times 10^{-6}$	$4.4694 \times 10^{-12}$
$50 \times 10^{-6}$	$2.1889 \times 10^{-9}$

The amount of error is propagated in simulation results; and as a result, the greatest error occurs in renal artery (according to Table 5).

Figs. 6(a and b) demonstrate the pressure and wall shear stress (WSS) contours at systole when are applied the non-Newtonian results of the pore network model. Considering WSS distribution, after the branching flows of the renal arteries, the main flow pattern is less complicated due to its high flow rate ratio into

the iliac arteries. This phenomena was also demonstrated by Lee and Chen [36]. Similar to the WSS distribution, the results of pressure is consistent with the finding of Mabotuwana et al. [37] where an average pressure of 13kPa was reported at systole along the abdominal artery. Moreover, a visual comparison between pressure drop in renal arteries and the main artery shows that resistance due to the presence of organ is much higher than the vascular resistance.

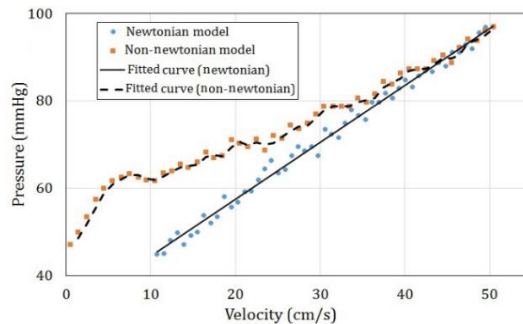


Fig. 5. Inlet pressure to the renal tissue versus inlet velocity calculated by pore network model.

Table 3. Constant parameters of Eq. (12).

Parameter	Value	Parameter	Value	Parameter	Value
$a_1$	112	$b_1$	0.04884	$c_1$	-0.2831
$a_2$	34.02	$b_2$	0.0992	$c_2$	1.358
$a_3$	7.178	$b_3$	0.4468	$c_3$	-9.6
$a_4$	7.371	$b_4$	0.4666	$c_4$	1.897
$a_5$	1.246	$b_5$	0.6495	$c_5$	-1.285

Table 4. Comparison between predicted permeability by the presents pore network model and experimental data in different velocity of renal artery.

Blood velocity (cm/s)	Experimental pressure (mmHg)*	Predicted pressure, Newtonian model (mmHg)	Predicted pressure, non-Newtonian model (mmHg)	Error, Newtonian model (%)	Error, non-Newtonian model (%)
10.75	51.91	45.35	46.64	12.63	10.16
17.35	62.72	53.96	62.80	13.96	0.13
23.95	67.16	62.57	68.21	6.84	1.56
30.55	71.58	71.18	72.20	0.57	0.87
37.16	76.25	79.80	79.61	4.65	4.41
43.76	79.33	88.4	88.17	11.44	11.14
50.36	89.54	97.01	97.16	8.34	8.51

Average error, Newtonian model=8.35%

Average error, non-Newtonian model=5.25%

\*Mills et al. 1970

Table 5. Comparison of velocity and pressure results obtained by the present work and experimental measurements.

Parameter	Experimental value*	Simulated results	Percentage of error
Velocity in renal artery	48.66(cm/s)	42.75(cm/s)	12.14%
Velocity in descending aorta	78.5(cm/s)	73.5(cm/s)	6.34%
Velocity in abdominal aorta	64.8(cm/s)	60.5(cm/s)	6.64%
Pressure in renal artery	83.3(mmHg)	85(mmHg)	2.04%
Pressure in descending and abdominal aorta	99(mmHg)	101(mmHg)	2.02%

\*Mills et al. 1970

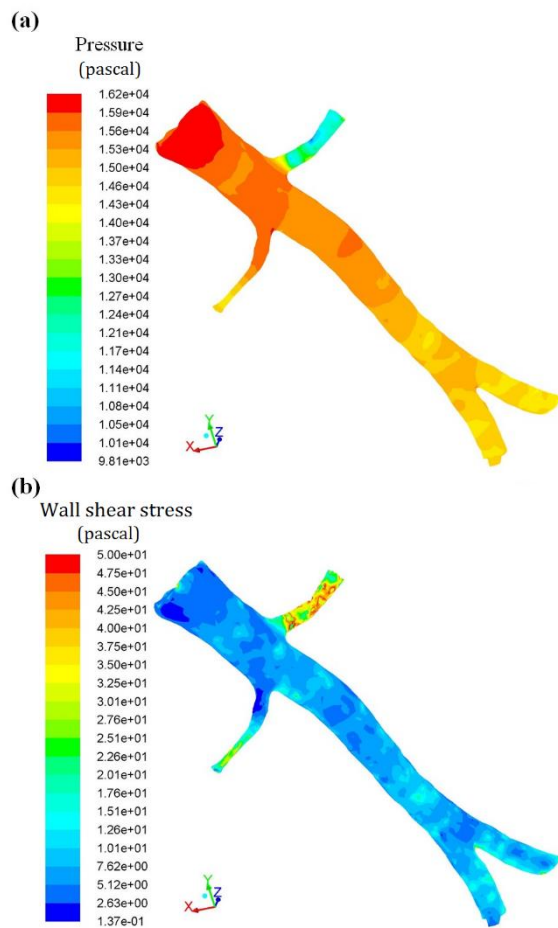


**Fig. 6.** Contours of (a) pressure and (b) wall shear stress along the arterial wall at systole instance.

**4. Conclusions**

The three-dimensional simulations of a patient specific aorta provide various types of information which are useful for medical practitioners. However, few studies have been undertaken to overcome the weak aspects of three-dimensional studies especially in terms of the proper outlet boundary condition. In this study, a three-dimensional patient specific abdominal aorta model was constructed. One important aspect of this study is that organs or body parts were modeled as porous media and the results are applied as the outlet boundary condition where blood flow/organ interactions occur. As a result, it was obtained three dimensional detailed and realistic flow and pressure distribution. Thus the liver tissue was simulated as a 3D porous medium using the pore

network model. Body organs are simulated by the method for the first time. Model parameters including the number of nodes, coordination number and the average pore radius, were set according to the experimental data of liver. Moreover, the modeling was performed assuming both Newtonian and non-Newtonian blood rheology. The results indicated that a network with 40 nodes, coordination number 5 and average pore radius  $3.3 \times 10^{-6}m$  mimics the actual liver tissue. Additionally, the Carreau-Yasuda non-Newtonian model predicts permeability more accurately than the Newtonian model. Finally, a comparative study on the inlet pressure to the renal pressure, between developed model and experimental data, showed that the pore network model can satisfyingly estimate the relation between pressure and velocity. And the results are used as the outlet boundary condition in abdominal aortic blood flow simulation. In general, the obtained results were consistent with those of the earlier studies. In addition, the current pore network model with less modifications can be extended to the simulation of other arterial flows considering flow-organs interactions.

**References**

- [1] A. D. Caballero and S. Lain, “A Review on Computational Fluid Dynamics Modelling in Human Thoracic Aorta”, *Cardiovascular Eng. Technol.*, Vol. 4, No. 2, pp. 103-130, (2013).
- [2] J. Y. Park, C. Y. Park, C. M. Hwang, K. Sun and B.G. Min, “Pseudo-organ boundary conditions applied to a computational fluid dynamics model of the human aorta”, *Comput. Biol. Med.* , Vol 37, No. 8, pp. 1063-1072, (2007).
- [3] A. C. Benim, A. Nahavandi, et al., “Simulation of blood flow in human aorta with emphasis on outlet boundary conditions”, *Appl. Math. Modell.*, Vol 35, No. 7, pp. 31753188, (2011).
- [4] E. O. Kung, A. S. Les, et al., “In vitro validation of finite element model of AAA hemodynamics incorporating realistic outlet boundary conditions”, *J. Biomech. Eng.*, Vol. 133, No. 4, pp. 041003, (2011).
- [5] I. E. Vignon-Clementel, C. A. Figueroa, K. E. Jansen and C. Taylor, “Outflow boundary conditions for three dimensional finite

- element modelling of blood flow and pressure in arterries”, *Comput. Methods Appl. Mech. Eng.*, Vol. 195, No. 29-32, pp. 37763796, (2006).
- [6] A. B. Deoghare, “Modelling of Human Abdominal Artery for Blood flow Analysis”, *Mater. Today: Proc.*, Vol. 5, No. 5, pp. 12877-12885, (2018).
- [7] M. Oshima, R. Torii, et al., “Finite element simulation of blood flow in the cerebral artery”, *Comput. Methods Appl. Mech. Eng.*, Vol. 191, No. 6-7, pp. 661-671, (2001).
- [8] C. A. Taylor, T. J. R. Hughes and C. K. Zarins, “Finite element modelling of blood flow in arteries”, *Comput. Methods Appl. Mech. Eng.*, Vol. 158, No. 1-2, pp. 155-196, (1998).
- [9] M. Borse, S. Bhushan, D. Walters, G. Burgreen, “Numerical simulations of flow pattern and particle trajectories in feline aorta for hypertrophic cardiomyopathy heart conditions”, *Eng. Appl. Comput. Fluid. Mech.*, Vol. 12, No. 1, pp. 57-73, (2018).
- [10] J. Renner, R. Gardhagen, et al., “A method for subject specific estimation of aortic wall shear stress”, *WSEAS Trans. Biol. Biomed.*, Vol. 6, No. 3, pp. 49-57, (2009).
- [11] F. N. V. d. Vosse, J. D. Hart, et al., “Finite element based computational methods for cardiovascular fluid structure interaction”, *J. Eng. Math.*, Vol. 47, No. 3-4, pp. 335-368, (2003).
- [12] D. Gallo, G. D. Santis, et al. “On the use of in vivo measured flow rates as boundary conditions for image-based hemodynamic models of the human aorta: implications for indicators of abnormal flow”, *Ann. Biomed. Eng.*, Vol. 40, No. 3, pp. 729-741, (2012).
- [13] N. Shahcheraghi, H. A. Dwyer, A. Y. Cheer, A.I. Barakat and T. Rutaganira, “Unsteady and three-dimensional simulation of blood flow in the human aortic arch”, *J. Biomech. Eng.*, Vol. 124, No. 4, pp. 378-387, (2002).
- [14] E. Shalman, M. Rosenfeld, E. Dgany and S. Einav, “Numerical modeling of the flow in stenosed coronary artery. The relationship between main hemodynamic parameters”, *Comput. Biol. Med.*, Vol. 32, No. 5, pp. 329-344, (2002).
- [15] H. J. Kim, I. E. Vignon-Clementel, et al., “On coupling a lumped parameter heart model and a three-dimensional finite element aorta model”, *Ann. Biomed. Eng.*, Vol. 37, No. 11, pp. 2153-2169, (2009).
- [16] M. Dadvar, M. Sohrabi and M. Sahimi, “Pore network model of deactivation of immobilized glucose isomerase in packed-bed reactors I: Two-dimensional simulations at the particle level”, *Chem. Eng. Sci.*, Vol. 56, No. 8, pp. 2803-2819, (2001).
- [17] M. Dadvar and M. Sahimi, “The effective diffusivities in porous media with and without nonlinear reactions”, *Chem. Eng. Sci.*, Vol. 62, No. 5, pp. 1466-1476, (2007).
- [18] M. Dadvar and M. Sahimi, “Pore network model of deactivation of immobilized glucose isomerase in packed-bed reactors. Part III: Multiscale modelling”, *Chem. Eng. Sci.*, Vol. 58, No. 22, pp. 4935-4951, (2003).
- [19] M. Dadvar and M. Sahimi, “Pore network model of deactivation of immobilized glucose isomerase in packed-bed reactors II: three-dimensional simulation at the particle level”, *Chem. Eng. Sci.*, Vol. 57, No. 6, pp. 939-952, (2002).
- [20] E. N. Marieb and K. Hoehn, *Anatomy and physiology*, 3<sup>rd</sup> ed., San Francisco, (2008).
- [21] C. Debbaut, J. Vierendeels, et al., “Perfusion characteristics of the human hepatic microcirculation based on 3D reconstructions and computational fluid dynamic analysis”, *J. Biomech. Eng.*, Vol. 134, No. 1, pp. 011003-011010, (2012).
- [22] S. Karimi, M. Dabagh, P. Vasava, M. Dadvar, B. Dabir and P. Jalali, “Effect of rheological models on the hemodynamics within human aorta”, *J. Non-Newtonian Fluid Mech.*, Vol. 207, pp. 42-54, (2014).
- [23] J. Boyd, J. M. Buick and S. Green, “Analysis of the Casson and Carreau-Yasuda non-Newtonian blood models in steady and oscillatory flows using the lattice Boltzmann method”, *Phys. Fluids*, Vol. 19, No. 9, pp. 093103, (2007).
- [24] G. P. Biro, “Comparison of acute cardiovascular effects and oxygen-supply following haemodilution with dextran, stroma-free haemoglobin solution and fluorocarbon suspension”, *Cardiovasc. Res.*, Vol. 16, No. 4, pp. 192-204, (1982).
- [25] E. W. Merrill, “Rheology of blood”, *Physiol. Rev.*, Vol. 49, No. 4, pp. 683-888, (1969).
- [26] R. Skalak, S.R. Keller and T.W. Secomb, “ASME centennial historical perspective paper: mechanics of blood flow”, *J. Biomech. Eng.*, Vol. 103, No. 2, pp. 102-115, (1981).
- [27] R. B. Bird, W. E. Stewart, E. N. Lightfoot, *Transport phenomena*, John Wiley & Sons, (2007).

- [28] J. E. Moore and D. N. Ku, "Pulsatile velocity measurements in the model of human abdominal aortic under simulated exercise and postprandial conditions", *J. Biomech. Eng.*, Vol. 116, No. 1, pp. 107-111, (1994).
- [29] T. Shipkowitz, V. G. Rodgers, J. Lee and K.B. Chandran, "Numerical study on the effects of secondary flow in the human aorta on the local shear stresses in the abdominal aortic branches", *J. Biomech.*, Vol. 33, No. 6, pp. 717-728, (2000).
- [30] S. M. A. Khader, et al., "Haemodynamics Behaviour in Normal and Stenosed Renal Artery using Computational Fluid Dynamics", *J. Adv. Res. Fluid Mech. Therm. Sci.*, Vol. 51, No. 1, pp. 80-90, (2018).
- [31] C. C. Botar, Á.Á. Tóth, et al., "Dynamic simulation and Doppler Ultrasonography validation of blood flow behavior in Abdominal Aortic Aneurysm", *Phys. Med.*, Vol. 37, pp. 1-8, (2017).
- [32] D. Elad, S. Einav, *Physical and flow properties of blood*, McGraw-Hill Companies, (2009).
- [33] C. J. Mills, I. T. Gabe, et al., "Pressure-flow relationships and vascular impedance in man", *Cardiovasc. Res.*, Vol. 4, No. 4, pp. 405-417, (1970).
- [34] A. A. Soares, S. Gonzaga, C. Oliveira, A. Simões, A.I. Rouboa, "Computational fluid dynamics in abdominal aorta bifurcation: non-Newtonian versus Newtonian blood flow in a real case study", *Comput. Meth. Biomech. Biomed. Eng.*, Vol. 20, No. 8, pp. 822-831, (2017).
- [35] F. Abdulrahim, "A Three-Dimensional Transient Numerical Study and Analysis of Blood Flow Dynamics in Renal Artery Aneurysms", University of Central Oklahoma, (2017).
- [36] D. Lee and J. Y. Chen, "Numerical simulation of steady flow fields in a model of abdominal aorta with its peripheral branches", *J. Biomech.*, Vol. 35, No. 8, pp. 1115-1122, (2002).
- [37] T. Mabotuwana, L. K. Cheng and A. J. Pullan, "A model of blood flow in the mesentric arterial system", *Biomed. Eng. Online*, Vol. 6, No. 1, pp. 17-29, (2007).

Copyrights ©2021 The author(s). This is an open access article distributed under the terms of the Creative Commons Attribution (CC BY 4.0), which permits unrestricted use, distribution, and reproduction in any medium, as long as the original authors and source are cited. No permission is required from the authors or the publishers.



### How to cite this paper:

S. Karimi, M. Dadvar and B. Dabir, "Simulation of blood flow in the abdominal aorta considering penetration into the organs using pore network model", *J. Comput. Appl. Res. Mech. Eng.*, Vol. 10, No. 2, pp. 437-447, (2021).

**DOI:** 10.22061/jcarme.2020.5882.1747

**URL:** [https://jcarme.sru.ac.ir/?\\_action=showPDF&article=1223](https://jcarme.sru.ac.ir/?_action=showPDF&article=1223)

